Silicon (2021) 13:4381–4389
https://doi.org/10.1007/s12633-020-00755-0

ORIGINAL PAPER

# Characterization and Properties of Sodium Hexa-Fluorosilicate and its Potential Application in the Production of Sodium Fluoride

Farzin Arianpour[1] · Aslı Çakır Arianpour[2] · Behnam Aali[3]

Received: 6 August 2020 / Accepted: 29 September 2020 / Published online: 12 October 2020


## Abstract

Sodium hexa-fluorosilicate ($Na_2SiF_6$) is a synthetic inorganic material with distinguished chemical, thermal and optical properties. In this research, a pure sodium hexa-fluorosilicate sample was systematically investigated via various characterization techniques. The amounts of constitutional elements and impurities were investigated using X-ray fluorescence and the chemical purity was determined as 99.89 wt%. Physical properties were calculated as 2.7085 g/cm$^3$ for density, 0.98 m$^2$/g for specific surface area and a mean particle size ($D_{50}$) of 77.3 μm. Thermal analysis was applied to understand the degradation of $Na_2SiF_6$ till 900 °C. The mineral composition and morphology was studied using X-ray diffraction, scanning and transmission electron microscopy and revealed the existence of P321 type hexagonal structure associated by elongated prism shaped precipitated crystals. Spectroscopy studies were performed via different techniques at different ranges of measurement. Thermal stability was investigated by post-mortem phase analysis of heat treated $Na_2SiF_6$ samples and showed a well stability till 400 °C. It is proposed that the thermal dissociation of $Na_2SiF_6$ can be utilized as a facile, inexpensive and green way for the synthesis of sodium fluoride instead of routine hydrofluoric acid-based methods. The obtained results suggested that the examined sodium hexa-fluorosilicate material could potentially be used as a reliable precursor in the synthesis of fluoride and silicon based materials due to its acceptable physical properties, chemical purity and thermal behavior.

**Keywords** Sodium hexa-fluorosilicate · Sodium fluoride · Thermal analysis · X-ray characterization · Spectroscopy · Microstructure

## 1 Introduction

Hexa-fluorides are composed of various fitted elements in the general formula of $A_xB_yF_6$ with superior physical, chemical and electronic properties [1, 2]. Sodium hexa-fluorosilicate ($Na_2SiF_6$), also known as sodium hexa-fluosilicate and sodium silicofluoride, is a typical ternary hexa-fluoride with some specific applications in ceramic, chemical and electronic industries thanks to its distinguished chemical, physical and optical properties [3]. It is industrially produced by neutralization and precipitation of hexa-fluorosilicic acid ($H_2SiF_6$) using sodium salts (e.g. hydroxide, carbonate, chloride or sulfate) under vigorous agitation according to the Eq. 1 [4].

$$SiF_6^{2-} + 2\ Na^+ \rightarrow Na_2SiF_6 \quad (1)$$

Crystallization of sodium hexa-fluorosilicate occurs immediately when reactants are mixed and therefore the reaction time is very short. The precipitated product is removed by filtration followed by water washing and drying at 150 °C [3, 5]. The conversion type depends on the hexa-fluorosilicic acid concentration and amounts of neutralization materials. Highly pure $Na_2SiF_6$ materials are produced in laboratory scale via similar method using various types of starting materials [6]. It is also possible to synthesize doped $Na_2SiF_6$ materials with different electronic, optical and luminescence properties [7–9]. $Na_2SiF_6$ is soluble in ether and acids and weak soluble in alcohols and water [3, 4]. It decomposes in alkaline solutions and produces sodium fluoride (NaF) and silicon oxide ($SiO_2$).

✉ Farzin Arianpour
farianpour@kastamonu.edu.tr

[1] Research and Application Center, Kastamonu University, Kastamonu, Turkey

[2] Department of Ceramic and Glass, Faculty of Fine Arts and Design, Kastamonu University, Kastamonu, Turkey

[3] Research & Development Center, Arya Tabalvor Arvand Co, Abadan, Iran

$Na_2SiF_6$ is mainly applied as a potential fluorine source in fluorination of municipal water, pharmaceutical and health-care products [1]. Due to the high amount of fluorine, it shows good antiseptic and preservative properties and used in wood, leather, textile, paper, rubber, insecticide, and pesticide industries [10]. $Na_2SiF_6$ is also utilized as an additive in cements and concretes [11], ore refining and beneficiation [12], phosphate industry [13], water oxidation [14], molten salt process [15], polymer composite [16] and dental materials [17]. Thanks to low melting temperature and fluxing activity, $Na_2SiF_6$ is applied in aluminum casting [18], silicon production [19], metal recovery [20] and corrosion protective coatings [21]. It is also used in ceramic industry as opacifier in opal glasses [22], glass production [23], and vitreous enamels [24]. $Na_2SiF_6$ is applied as a potential precursor in the synthesis of silicon-based ceramics such as silica [25] and silicon nitride [26] via heating under controlled atmospheres. Fluoride materials (e.g. NaF, $AlF_3$, $MgSiF_6$, and cryolite) could also be synthesized using $Na_2SiF_6$ as starting material. $Na_2SiF_6$ was successfully used in meta-kaolin based geopolymers as an additive to enhance the mechanical strength [27]. Due to distinguished optical and luminescence properties, it has recently found some advanced applications in microelectronics, semiconductors, optoelectronic devices, catalysts, photonics and nonlinear optical materials [28–31]. Sodium hexa-fluorosilicate is a promising material in the white LED application as a superior solid state lightening source. Due to its high efficiency, energy saving and environmentally issues, this product is used in the lightening, decoration, and electronic. It is known that fluoride ion doping can enhance the luminescence properties of the silicate phosphors which lead to the new generation of promising luminescent products as fluorosilicate phosphors [32–34].

Although sodium hexa-fluorosilicate is utilized in some applications, to the best of our knowledge, some characteristics of this material were not investigated comprehensively before. The aim of this study is the characterization of a pure available sodium hexa-fluorosilicate powder in terms of chemistry, physical properties, thermal behavior, phase and microstructural features as well as spectroscopy analyses. The thermal dissociation of $Na_2SiF_6$ is also investigated as a facile, inexpensive and environmentally friendly route for the synthesis of sodium fluoride instead of conventional hazardous hydrofluoric acid-based methods.

## 2 Materials and Methods

### 2.1 Raw Material

Sodium hexa-fluorosilicate (ATA Chem. Co., Iran) was provided as a white granules (50–400 μm) with a purity of >99.2%, according to the manufacturer. The as-received sample was used in characterizations without furthered chemical purification. Before tests, it was oven dried at 105 °C for 12 h and then, light-milled using an agate mortar to break the large agglomerates. The sample was finally passed through a 210 μm sieve to obtain a homogeneous fine powder.

### 2.2 Characterization

Chemical composition was investigated via X-ray fluorescence (XRF). Test pellet was prepared by mixing of 4 g $Na_2SiF_6$ and 0.9 g analytical grade wax and pressing into a 32 mm die using a manual hydraulic press. The pellet was subjected to X-ray on a Xepos III machine (Spectro, Germany) equipped with a Pd anode X-ray tube. Powder density was measured by gas pycnometry on an Upyc 1200e pycnometer system (Quantachrome, USA) using pure He gas (99.99%) at ambient temperature. The test was repeated for 5 times and the average value was reported. Particle size distribution was investigated by a HELOS H2396 (Sympatec, Germany) laser diffraction system. Previously, 10 mg of $Na_2SiF_6$ powder was dispersed in 100 mL of distilled water via stirring at 1000 rpm rate under ultra-sonication. Specific surface area was measured based on $N_2$-physisorption and Brunauer-Emmett-Teller (BET) method on a NOVATOUCH (Quantachrome, USA) system using ultra-pure nitrogen gas at 77 K. The sample was previously degassed to release the adsorbents by heating (10 °C/min, 3 h holding at 150 °C) under vacuum (6 mmHg/s evacuating rate and final pressure of 250 μmHg). Thermal analysis (thermo-gravimetry (TG), differential thermo-gravimetry (DTG) and differential scanning calorimetry (DSC)) was conducted on a STA 449F3 machine (Netzsch, Germany). Approximately 25 mg of $Na_2SiF_6$ sample was poured in an alumina cell and heated up to 900 °C with a heating rate of 5 °C/min under nitrogen flow of 30 $cm^3$/min. Phase composition was investigated by X-ray diffractometery (XRD) on a D8 Advance diffractometer (Bruker, USA) using Ni-filtered Cu $K_{\alpha 1}$ radiation ($\lambda$ = 1.5406 Å) and generator setting of 40 kV and 40 mA. Pattern was measured in $2\theta$ range of 10-80°, step size of 0.02° and 1.5 s counting time per step at room temperature. Constitutional phases were identified via EVA software supported by a Powder Diffraction File (PDF) data base. The crystallite sizes were measured for 5 most intense peaks according to the Scherrer's formula (Eq. 2),

$$L = k\,\lambda / B\,\mathrm{Cos}\,(\theta) \tag{2}$$

where, $L$ is the crystallite size (in nm), k is the Scherrer constant (0.94), $\lambda$ is the X-ray wavelength (1.5406 Å), $\theta$ is the Bragg angle, and $B$ (in rad.) is full-width at half-maximum intensity of diffraction peaks. $B$ was taken as the experimental full width ($B_{exp}$) and corrected for the experimental instrumental broadening ($B_{ins}$) according to the Eq. 3.

$$B = \left(B_{exp}^2 - B_{ins}^2\right)^{1/2} \tag{3}$$

$B_{ins}$ was measured experimentally using a standard silicon diffraction sample [35]. Microstructure and morphology was characterized using a FEG 250 field emission scanning electron microscope (FE-SEM, QUANTA, Czech) equipped with an EDAX energy dispersive spectroscope (AMETEC, USA). For SEM observations, small amount of $Na_2SiF_6$ sample was dispersed in distilled water, spread on a carbon bond, air dried and then gold-platinum coated with a sputtering system (Cressington, UK) to prevent electron charge. High resolution transmission electron microscopy (HR-TEM) was performed using a JEM 2100 UHR (JEOL, Japan) system working at 200 kV equipped with a $LaB_6$ electron gun. TEM sample was prepared by ultrasound dispersion of $Na_2SiF_6$ powder into isopropanol, putting a small drop onto a 200 mesh copper grid and covering by an amorphous carbon film. The micrographs have been taken in the bright field (BF) mode. All length measurements on the microstructural figures were done using ImageJ, a Java-based image processing program developed at the National Institutes of Health and the Laboratory for Optical and Computational Instrumentation (LOCI, University of Wisconsin). Fourier transform infrared (FT-IR) spectroscopy was performed on an Alpha Platinum-ATR (Bruker, USA) system equipped with a single reflection diamond crystal. Approximately 0.1 mg of $Na_2SiF_6$ sample poured on the holder and fixed by pressing the head. The spectrum was recorded in the range of 4000–300 $cm^{-1}$ by resolution of 3 $cm^{-1}$ after 64 scans at room temperature. UV-VIS-NIR spectrum was measured on a 3600 spectrophotometer (Shimadzu, Japan). The specular reflection results were recorded in the wavelength range of 220–1500 nm at room temperature. Raman spectrum was obtained using a confocal Raman microscope (inVia, Renishaw, UK) equipped with a 532 nm excitation laser source in the range of 150–1000 $cm^{-1}$ at room temperature.

## 3 Results and Discussion

### 3.1 Chemical Analysis

Table 1 lists the main constitutional elements of the $Na_2SiF_6$ sample which was measured using XRF analysis. As it shows, the main elements are composed of Na (24.43 wt%), Si (14.91 wt%) and F (60.54 wt%) which are close to the theoretical values of 24.47, 14.89 and 60.64 wt% for Na, Si and F, respectively. The detected impurity elements are determined as Fe, Al, Ca, and Mg with the total amount of <0.11 wt% and are probably generated from the used raw materials or entered during processing. The contents of the toxic elements such as heavy metals (Pb, Ni, Cr, etc.) seem to be very low which were not detectable by XRF method. However the high purity (99.89 wt%) and low impurity content would make this sample to be considered in some healthcare applications such as fluorination of water [36].

### 3.2 Physical Properties

Table 1 lists the physical properties of $Na_2SiF_6$ powder including density, specific surface area and particle size distribution. The measured powder density of $Na_2SiF_6$ using helium gas pycnometry is equal to 2.71 $g/cm^3$ which is close to the theoretical value of 2.70 $g/cm^3$. The volume measured in gas pycnometry technique is considered as the finest scale of three-dimensional spaces and surface roughness which depends on the atomic size of the applied injected gas. Therefore, the volume measured using helium is often prescribed as a reliable value for powder materials due to the small size and inertness of the He gas [37]. According to $N_2$-physisorption measurement and BET method, the specific surface area of $Na_2SiF_6$ was measured as 0.96 $m^2/g$ which shows a low value for this inorganic synthetic material. Gas physisorption technique is a helpful measuring rout for the overall surface of powder particles including inter-particular pores. However, it does not measure the volume of sealed pores, unlike quantitative microscopy techniques which measure both open and closed porosities. This low value of BET proves that the property of $Na_2SiF_6$ powder is dominated by bulk rather than surface of material [38]. The particle size distribution of $Na_2SiF_6$ sample was investigated via laser diffraction and the summary of results is reported in Table 1.

Figure 1 also shows the cumulative distribution and histogram curves of particles. Static laser diffraction analysis is a fast, feasible, convenient, and non-destructive rout to determine the particle size distribution of inorganic powders by measuring the scattering angle and intensity of laser after passing through a diluted particle dispersions suspended in a proper liquid [39]. Due to the low solubility of $Na_2SiF_6$, water was selected as dispersion media and the combination of stirring

**Table 1** Chemical analysis and physical properties of $Na_2SiF_6$

| Element | Na | Si | F | Fe | Al | Ca | Mg | Sum. |
|---|---|---|---|---|---|---|---|---|
| Wt% | 24.43 | 14.91 | 60.55 | 0.05 | 0.03 | 0.02 | 0.01 | 100 |
| Density ($g/cm^3$) | | Specific surface area ($m^2/g$) | | | | Particle size distribution (μm) | | |
| | | | | | | $D_{10}$ | $D_{50}$ | $D_{90}$ |
| 2.7085 | | 0.98 | | | | 38.7 | 77.3 | 120.97 |

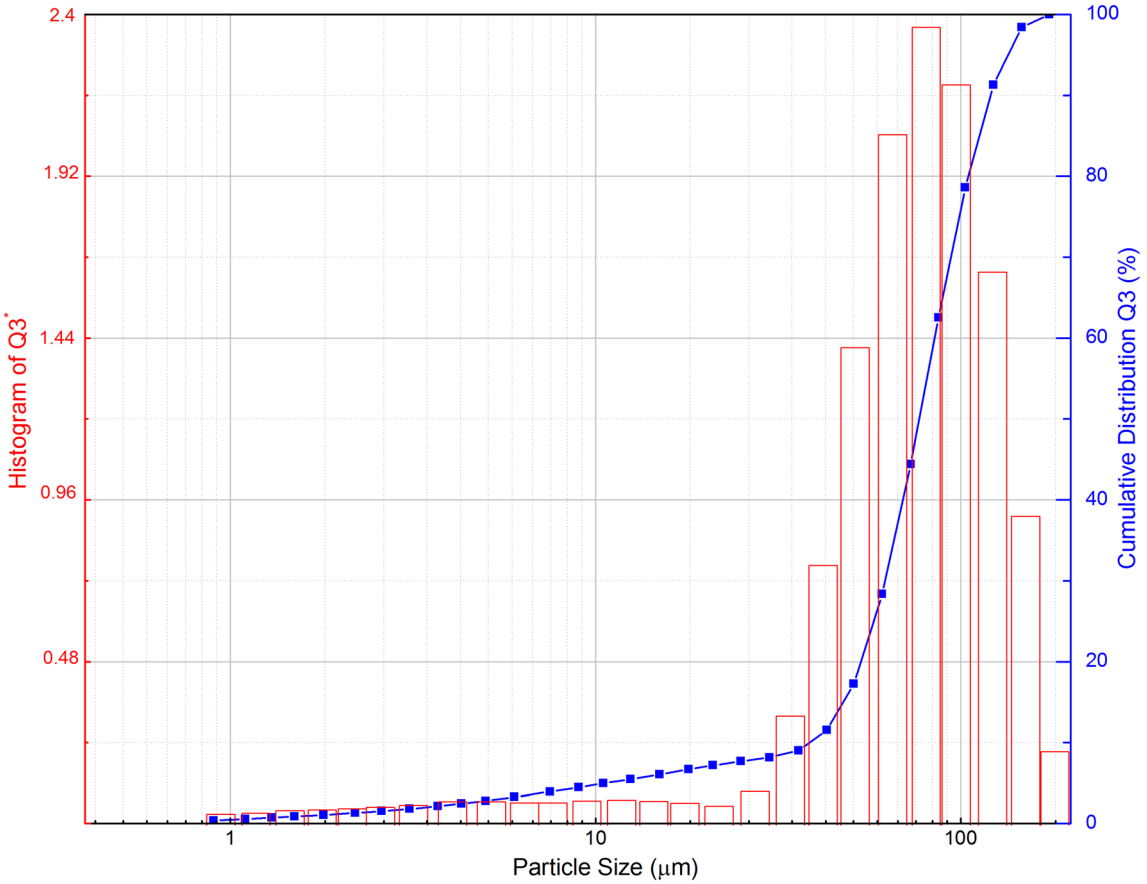


**Fig. 1** Particle size distribution of $Na_2SiF_6$

and ultra-sonication would allow the sufficient time for disagglomeration of particles. It reveals that the particle size of $Na_2SiF_6$ sample is in the range of 38–121 μm with the average size of 77 μm. Type of the used raw materials and the applied synthesis process have strong effects on particle growth and size distribution of the final $Na_2SiF_6$ powder. The nucleation and growth of $Na_2SiF_6$ particle immediately happen in the solution during precipitation synthesis. After calcination process, particles could join to form larger angular shaped aggregates. The particle morphology will be discussed later in the microstructural analysis section.

### 3.3 Thermal Behavior

Figure 2 shows the thermal analysis curves (DSC/TG/DTG) of the $Na_2SiF_6$ sample after heating up to 900 °C under $N_2$ atmosphere. As this figure shows, till 400 °C, there is no important peak in the thermal analysis curves due to structural stability of $Na_2SiF_6$ sample. Small mass loss (0.23 wt%) till 400 °C reveals a complete dehydration of powder and may attributed to the removal of the absorbed water molecule from the environment. According to the TG curve, the decomposition of $Na_2SiF_6$ is gradually started around 428 °C and ended at 575 °C with a clear endothermic reaction accompanied with a huge amount of mass loss (54.02 wt%). The temperature of the maximum dissociation phenomena was determined as 556.2 °C and 556.5 °C corresponding to the sharp endothermic peaks in the representative DSC and DTG curves, respectively. Sodium hexa-fluorosilicate is decomposed to sodium fluoride (NaF) and silicon tetrafluoride ($SiF_4$) by heating over 500 °C according to the Eq. 4 [40, 41].

$$Na_2SiF_{6(s)} \rightarrow 2NaF_{(s)} + SiF_{4(g)} \quad (4)$$

$NaF_2$ is a stable solid salt which would remain after decomposition reaction; while, $SiF_4$ is a gas which removes into atmosphere. This gas removal leads to the observed 54.02 wt% mass loss which is close to the theoretical value of 55.32 wt%. Depending on the particle size, presence of the impurities, applied heating rate and atmosphere, the decomposition temperature of $Na_2SiF_6$ may slightly shift to lower or higher temperatures. Thermal decomposition of $Na_2SiF_6$ was also reported that happened at 500 °C in air [32] and 450–580 °C with 55.9 wt% mass loss in argon [28]. Thermal behavior and decomposition temperature are momentous issues in some applications of $Na_2SiF_6$ powder as raw material, e.g. in opal glass, glass-ceramic, glaze and frit production due to the high temperatures of processing [22]. It is also an

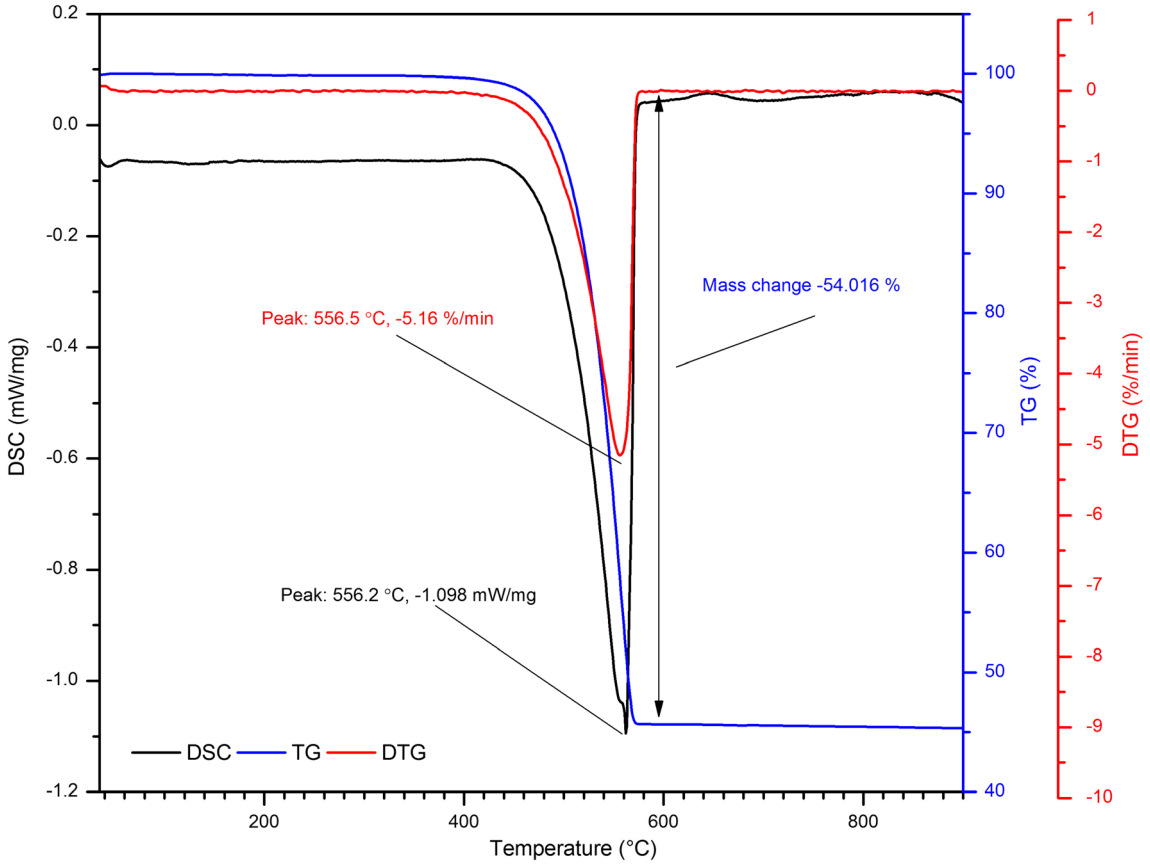


**Fig. 2** Thermal analysis (DSC/TG/DTG) curves of $Na_2SiF_6$

inexpensive green way for the production of NaF without using HF. Likewise; this phenomenon was applied in the synthesis of mesoporous silica and silicon nitride materials under controlled atmosphere [25, 26]. The kinetic mechanism of $Na_2SiF_6$ dissociation was studied in some researches to reveal the effects of heating condition on reaction rate. Kashiwaya et al. determined a formula for the rate constant of dissociation as a function of temperature and the activation energy was calculated as 106.6 ± 0.7 kJ/mol over a temperature range of 427 to 1347 °C in gas phase [40]. In another work, the optimal processing condition of complete dissociation of $Na_2SiF_6$ was proposed as heating at 650 °C for 40 min under pure nitrogen atmosphere [42].

### 3.4 Phase Analysis

Figure 3 shows the representative X-ray diffraction pattern of $Na_2SiF_6$ samples after heating at different temperatures. To evaluate the phase evolution and dissociation behavior, according to thermal analysis test, $Na_2SiF_6$ powders were heated at 400, 500, 600 and 700 °C for 2 h in an electric resistance furnace in air. As this figure shows, for as-received $Na_2SiF_6$ powder, all peaks can be attributed to the Malladrite phase (sodium hexa-fluorosilicate, $Na_2SiF_6$) according to the relevant reference diffraction card (JCPDS# 00–033-1280). It can be said that the $Na_2SiF_6$ material shows a good crystallinity with a very few miscellaneous peaks in the X-ray diffraction pattern. Sodium hexa-fluorosilicate crystallize in a non-centro-symmetric (NCS) space group of P321 hexagonal crystal structure with the lattice parameters of a = b = 8.859 Å and c = 5.038 Å [43]. This crystal system is highly symmetric and composed of two independent regular $[SiF_6]^{2-}$ octahedrons with six $F^{1-}$ in contact to a single $Si^{4+}$ ion. Two crystallographically independent sodium cation ($Na^{1+}$) are placed on both corners of the octahedral. On the other hand, this octahedral structure is identified by six Si-F bonds [28]. In general, $Na_2SiF_6$ has a similar crystal structure to other ternary $A_xB_yF_6$ hexa-fluorides compounds such as $Na_2PdF_6$, $Na_2TiF_6$, $Na_2MnF_6$, $Na_2IrF_6$, $Li_2SiF_6$, $Na_2GeF_6$, $Na_2PtF_6$, and $Na_2RhF_6$ [43]. According to the crystal structure and cell parameters of $Na_2SiF_6$, the theoretical density is close to 2.74 g/cm$^3$ which is comparable to the measured value of the 2.708 g/cm$^3$ obtained from helium gas pycnometry.

Table 2 lists the X-ray diffraction data and top 5 major peaks of $Na_2SiF_6$ sample. The average crystallite size was measured equal to 46.89 nm according to the Scherrer's formula. As it was previously discussed, the presence of some metal impurities (Fe, Al, Ca and Mg) were characterized in the XRF chemical analysis of the studied $Na_2SiF_6$ sample which were probable generated from the used raw materials or

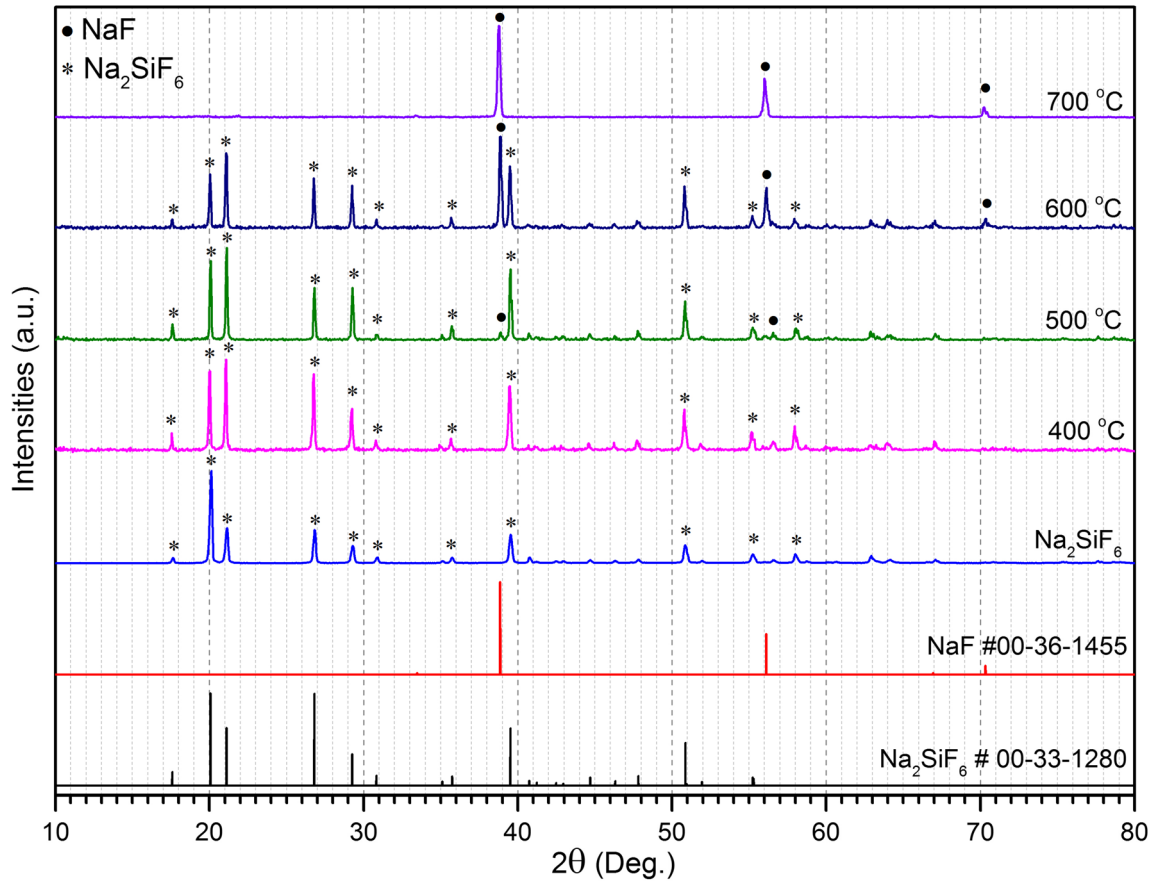


**Fig. 3** Representative X-ray diffraction patterns of as-received and heated $Na_2SiF_6$ samples

during production process. In the case of enough ion concentration and suitable ion substitution conditions (low differences in radius percentage (<15%) and electronegativity values), some cations can exchange the $Na^+$ position in the $Na_2SiF_6$ crystal structure. Depend on the radii difference, the d value of the inter-planar spacing changes and hence, the X-ray diffraction peaks would shift toward lower/higher angles of 2θ [32, 40, 44].

The X-ray diffraction patterns of heated $Na_2SiF_6$ samples at 400, 500, 600 and 700 °C for 2 h are also represented in Fig. 3. Based on the thermal analysis results (Fig. 2), the dissociation of $Na_2SiF_6$ was observed to be started at around 428 °C and ended at 575 °C with a clear endothermic peak at 556 °C. As this figure shows, heating at 400 °C for 2 h was not able to change the crystal structure of $Na_2SiF_6$ sample. At 500 °C, the formation of NaF crystals is slightly visible, while after heating at 600 °C, NaF seems to become the major phase in the related X-ray diffraction pattern according to the relevant reference diffraction card (JCPDS# 00–036-1455). It is obvious that heating at 700 °C totally decomposed the crystal structure of $Na_2SiF_6$ and the clear diffraction pattern of NaF is appeared. NaF is a white salt with a cubic crystal structure and melting point of 993 °C which is normally produced by neutralization of HF and served as an important fluorine source in pharmacology, medicine and chemistry [1]. The thermal dissociation of $Na_2SiF_6$ could be expected as an inexpensive eco-friendly route for the mass production of highly pure NaF.

**Table 2** X-ray diffraction data of as-received $Na_2SiF_6$ sample

| 2θ (deg.) | Intensity (%) | D (Å) | (hkl) | FWHM (rad.) | CS (nm) |
|---|---|---|---|---|---|
| 20.10 | 100 | 4.43 | (110) | 0.1765 | 47.74 |
| 21.14 | 38.2 | 4.21 | (101) | 0.1771 | 47.66 |
| 26.82 | 36.3 | 3.33 | (111) | 0.1855 | 45.98 |
| 39.53 | 31 | 2.28 | (301) | 0.2171 | 40.61 |
| 50.86 | 19.6 | 1.79 | (302) | 0.1751 | 52.47 |

### 3.5 Microstructural Features

Figure 4a-e show the microstructural features, morphology and point chemical analysis of the $Na_2SiF_6$ sample. According to the scanning electron micrographs (Figs. 4a-b), it is obvious that the $Na_2SiF_6$ aggregates are composed of some adhered hexagonal-shaped crystal prisms. The nucleation of prisms instantaneously happens after neutralization of $H_2SiF_6$ acid with sodium salts during precipitation synthesis. The crystal growth will be continued even after followed

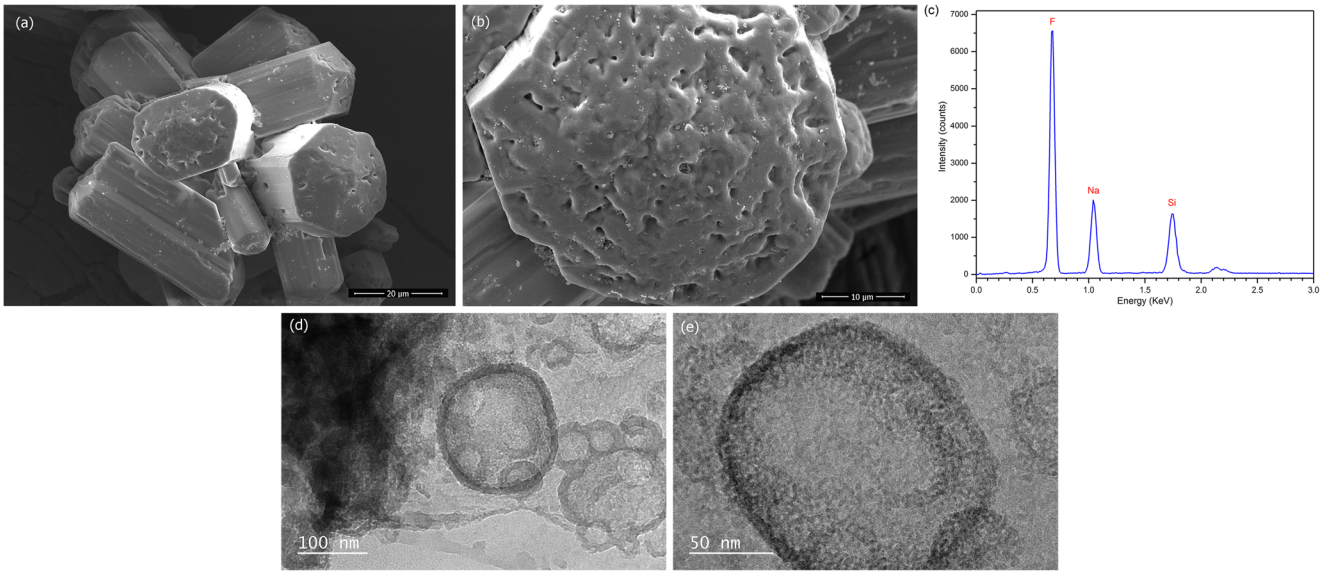


**Fig. 4** Microstructural features, morphology and point analysis of $Na_2SiF_6$ **a-b** scanning electron micrographs, **c** EDS spectrum and **d-e** high resolution transmission electron images

calcination process at the temperature of 180–250 °C for 2–5 h. As it was discussed before, $Na_2SiF_6$ is crystallized in hexagonal structure which leads to the formation of crystals as elongated hexagonal shaped prisms grown along c axis (basal plane (0001) of hexagonal crystal) [45]. As these figures show, the prisms have average dimensions of 35–50 µm in length and 15–20 µm in diameter according to the length measurements using ImageJ software. Figure 4b represents the cross section profile of a single $Na_2SiF_6$ prism and reveals the presence of some small pores with the diameter range of 1–3 µm. The pore formation assumed to be happened during water removal and dehydration after applied calcination process. Figure 4c shows the EDS point elemental analysis of the cross section profile of the represented prism in Fig. 4b. The representative amounts of Na, Si and F elements were measured equal to 33.2, 16.62 and 50.18 wt% which is comparable with the theoretical values of 24.47, 14.89 and 60.60 wt%, respectively. The impurity elements (Fe, Al, Ca and Mg) were not detected in the EDS spectra due to the lower amounts and sensitivity of the measurement. By comparison the elemental analysis results of XRF and EDS, it is clear that the obtained results from XRF are more close to the theoretical composition of $Na_2SiF_6$. Figures 4d-e show the high resolution transmission electron images of the $Na_2SiF_6$ sample. As it is visible, the $Na_2SiF_6$ material is essentially built up from oval shaped crystallites with the diameter sizes of 60–110 nm [32, 44]. Precipitation reaction is a general method in fast synthesis of insoluble nanomaterial species under high super-saturation condition. In this method, fast nucleation of particles is a key-point which leads to the formation of a large number of crystallites [46]. Precipitation is also a simple and rapid utilized route for $Na_2SiF_6$ synthesis in lab or industrial scale which happens instantaneously due to neutralization of hexa-fluorosilicic acid using various types of sodium salts. Concentration of starting materials, pH and applied heating regime of post-mortem calcination are the significant parameters which control the final morphology and grain size of $Na_2SiF_6$.

### 3.6 Spectroscopy

Figures 5a-c show the FT-IR, Raman and UV-Vis-NIR spectra of the $Na_2SiF_6$ powder. The FT-IR spectrum (Fig. 5a) was recorded in the range of 4000–300 $cm^{-1}$ and shows the specific absorption peaks at 472 and 705 $cm^{-1}$ which are attributed to the bending and tensile vibrations of $SiF_6^{2-}$ groups, respectively [44]. As this figure shows, the sharp and clear peaks of Si-F bonds are presented and there is not any trace of irrelevant vibrations in the spectrum. As it was reported elsewhere, in the presence of metal cation impurities in doped $Na_2SiF_6$ samples, a wide peak would be appeared in the range of 1250–1000 $cm^{-1}$ of the FTIR spectrum [32, 44]. This result is also in agreement with the X-ray diffraction data and proves that the studied $Na_2SiF_6$ powder is a nearly pure Malladrite phase. Similar observations were also reported by Zhang et al. [28] and Zhao et al. [32].

Figure 5b demonstrates the UV-Vis-NIR graph of the $Na_2SiF_6$ powder. The existence of the large electronegative F atom represents short transmission cutoff wavelengths in the UV spectrum of hexa-fluorosilicate materials [28]. The presented reflectance/absorption spectra exhibit that the studied $Na_2SiF_6$ material has no significant absorption in the range of 500 to 1500 nm. Below the 500 nm, by lowering the wavelength, the adsorption is increased rapidly and the reflectance is finally reduced to 65% at 220 nm. Figure 5c represents the Raman spectrum of the studied powder and shows the

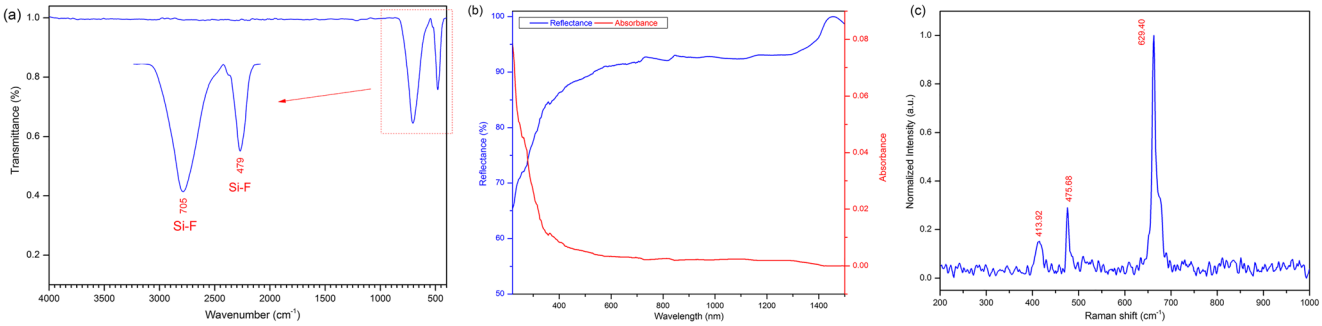


**Fig. 5** Spectral curves of $Na_2SiF_6$ **a** FT-IR, **b** UV-Vis-NIR and **c** Raman analysis

presence of major vibrating peaks at 629, 476 and 414 $cm^{1-}$ which are the main characteristic Raman band of $Na_2SiF_6$ material [32]. As there is no evidence of other non-related peaks, it seems that the studied $Na_2SiF_6$ material is a nearly pure hexagonal phase of Malladrite which is in agreement with Zhao et al. study [32]. In the presence of major impurity ions, the inhibition of the characteristic peaks or the signs of new local vibration modes may be appeared in the Raman spectra of $Na_2SiF_6$. It was reported that the characteristic peak of 476 $cm^{-1}$ could be slightly suppressed in the presence of impurity metal cations such as $Ce^{3+}$, $Tb^{3+}$ and $Eu^{3+}$ for doped synthesized $Na_2SiF_6$ samples [32].

## 4 Conclusions

A pure available sodium hexa-fluorosilicate ($Na_2SiF_6$) powder was deeply characterized via chemical, physical, thermal, phase, microstructural and spectral techniques. The XRF chemical analysis presented the purity of over 99 wt% and existence of Fe, Al, Mg and Ca as impurities. The physical properties measurements revealed the mean particle size ($D_{50}$) of 77.3 μm, density of 2.71 $g/cm^3$ and specific surface area of 0.98 $m^2/g^{-1}$. The mineralogical study via X-ray diffraction showed the presence of Malladrite phase, typical P321 hexagonal crystal structure and average crystallite size of 46.9 nm for as-received $Na_2SiF_6$ sample. The morphological studies using electron microscopies (FE-SEM/HR-TEM) revealed the presence of agglomerated particles consisting coherent semi-porous hexagonal shaped prisms elongated along c axis. The spectral analyses of as-received powder were also done via FT-IR, UV-Vis-NIR and Raman techniques at different ranges of measurement to disclose the molecular structure and bonding which proved the phase purity of the studied $Na_2SiF_6$ material. Thermal analysis study up to 900 °C under $N_2$ disclosed that the dissociation of $Na_2SiF_6$ gradually happens in the temperature range of 428–575 °C with a sharp endothermic peak at 556 °C associating by 54.02 wt% of mass loss. The XRD patterns of heated powders at different temperatures represented a good thermal stability of $Na_2SiF_6$ till 400 °C and completed dissociation and transformation to sodium fluoride at 700 °C which is in agreement with the thermal analysis results. Thermal dissociation of $Na_2SiF_6$ is shown to be a facile, eco-friendly and inexpensive method for the production of NaF instead of the conventional hydrofluoric acid-based methods.

**Acknowledgments** This work was supported by Scientific Research Project Coordination Unit of Kastamonu University (grant number KÜ-BAP01/2018-46).

## References

1. Lacson CFZ, Lu MC, Huang YH (2020) Fluoride network and circular economy as potential model for sustainable development - a review. Chemosphere 239:124662
2. Peresypkina EV, Blatov VA (2003) Structure-forming components in crystals of ternary and quaternary 3d-metal complex fluorides. Acta Cryst B59:361–377
3. Kumar M, Babu MN, Mankhand TR, Pandey BD (2010) Precipitation of sodium silicofluoride ($Na_2SiF_6$) and cryolite ($Na_3AlF_6$) from HF/HCl leach liquors of alumino-silicates. Hydrometallurgy 104:304–307
4. Toure AO, Sambe FM, Koita D, Diop CMG, Sock O (2012) Processes for working-up an aqueous fluosilicic acid solution. S Afr J Sci 108:1–5
5. Jeong HL, Huh YD (2010) Synthesis of hexagonal prisms and hexagonal plates of $Na_2SiF_6$ microcrystals. Mater Lett 64:1816–1818
6. Olchowka J, Suta M, Wickleder C (2017) Green synthesis of $A_2SiF_6$ (a=Li-Cs) nanoparticles using ionic liquids as solvents and as fluorine sources: a simple approach without HF. Chem Eur J 23:12092–12095
7. Barve RA, Patil RR, Moharil SV, Bhatt BC, Kulkarni MS (2016) Effect of $Al^{3+}$ co-doping on the luminescence properties of cu doped $Na_2SiF_6$. Appl Radiat Isotopes 116:57–62
8. Krylov VA, Sorochkina TG, Bulanov AD, Lashkov AY (2012) C1-C4 hydrocarbon release in the preparation of $SiF_4$ through $Na_2SiF_6$ pyrolysis. Inorg Mater 48:7–9
9. Valbe R, Maeorg U, Lohmus A, Reedo V, Koel M, Krumme A, Kessler V, Hoop A, Romanov AE (2012) A novel route of synthesis of sodium hexa fluorosilicate two component cluster crystals using $BF^{4-}$ containing ionic liquids. J Cryst Growth 361:51–56
10. Mukhamedyanov MM, Plotnikov IA (2014) Use of a chloroform by-product in raw fur and hide dressing processes. Russ Agric Sci 40:295–297
11. Wang H, Mao Q, Gao Y, Wang Z, Cui S (2017) Effect and mechanism of sodium fluosilicate on setting time of cement. Mater Sci Forum 898:1978–1983

12. Ren Z, Yu F, Gao H, Chen Z, Peng Y, Liu L (2017) Selective separation of fluorite, barite and calcite with valonea extract and sodium fluosilicate as depressants. Minerals 7:24
13. Rice CR, Slater C, Faulkner RA, Allan RL (2018) Self-assembly of an anion-binding cryptand for the selective encapsulation, sequestration, and precipitation of phosphate from aqueous systems. Angew Chem Int Ed 57:13071–13075
14. Natali M, Nastasi F, Puntoriero F, Sartorel A (2019) Mechanistic insights into light-activated catalysis for water oxidation. Eur J Inorg Chem 15:2027–2039
15. Cai Z, Li Y, Tian W (2011) Electrochemical behavior of silicon compound in LiF-NaF-KF-$Na_2SiF_6$ molten salt. Ionics 17:821–826
16. Chen G, Zhu S, Jiang Z, Gao L, Ma Z, Liu L (2017) Laser ablation protection of polymer matrix composites by adhesive inorganic coatings. J Mater Sci 52:12734–12741
17. Wiankowska KK, Lipa S, Krasowski M, Sokołowski J, Butkiewicz KL, Nowicka A (2020) Evaluation of gap formation at the composite resin-tooth interface after using universal adhesives: in vitro SEM study using the replica technique. Microsc Res Tech 83: 176–185
18. Shakhrai SG, Mikhalev YG, Kalinovskaya TG, Arkhipov GV, Ivanova AM (2016) Investigation and choice of materials for the electrical insulation of the steel bloom of an aluminum electrolyzer. Metallurgist 60:622–628
19. Spomer N, Holl S, Zherlitsyna L, Maysamy F, Frost A, Auner N (2015) Amorphous silicon: new insights into an old material. Chem Eur J 21:5600–5616
20. Frçhlich P, Lorenz T, Martin G, Brett B, Bertau M (2017) Valuable metals-recovery processes, current trends, and recycling strategies. Angew Chem Int Ed 56:2544–2580
21. Rehman ZU, Koo BH (2016) Combined effect of long processing time and $Na_2SiF_6$ on the properties of PEO coatings formed on AZ91D. J Mater Eng Perform 25:3531–3537
22. Vasconcelos HCSPM, Gonçalves MC (2016) Overall aspects of non-traditional glasses: synthesis, properties and applications. Bentham Sci Publishers:39–65
23. Khan MS, Shahzadi P, Alam S, Javed K, Shaheen F, Naqvi J, Shahnaz A (2015) Development of heat resistant borosilicate glass doped with sodium silico fluoride compound. J Chem Mater Res 4: 13–18
24. Kassem AS, Mostafa MZ, Abadir MF, Sherbiny SAE (2010) Hot water acid-resistant enamels for sheet steel. Mater Corrosion 61:58–63
25. Hui X, Gui L, Feng CJ, Ping LW (2014) Recovery of high specific area silica and sodium fluoride from sodium hexafluorosilicate. J Cent South Univ 21:4084–4090
26. Cruz ALL, Canul MIP (2007) In situ synthesis of $Si_3N_4$ in the $Na_2SiF_6$-$N_2$ system via CVD: kinetics and mechanism of solid-precursor decomposition. Solid State Ionics 177:3529–3536
27. Haddaji Y, Majdoubi H, Mansouri S, Tamraoui Y, Boulif R, Oumam M, Hannache H (2020) Effect of sodium hexafluorosilicate addition on the properties of metakaolin based geopolymers cured at ambient temperature. Silicon. https://doi.org/10.1007/s12633-020-00536-9
28. Zhang W, Jing Q, Fang Y, Chen Z (2017) Synthesis, structure and properties of nonlinear optical crystal $Na_2SiF_6$. Z Anorg Allg Chem 643:1739–1743
29. Ha J, Novitskaya E, Lam N, Sanchez M, Kim YH, Li Z, Im WB, Graeve OA, McKittrick J (2020) Synthesis of $Mn^{4+}$ activated $Na_2SiF_6$ red-emitting phosphors using an ionic liquid. J Lumin 218:116835
30. Liu Y, Li Y, Meng J, Liang W, Huang W, Liao S, Huang Y, Zhang H (2020) Novel luminescence enhancement and splitting of excitation and emission bands of $Na_2SiF_6$:$Mn^{4+}$,$Li^+$ phosphors induced by $Li^+$ co-doping. J Lumin 217:116770
31. Tiwari A, Dhoble SJ (2019) Tunable lanthanide/transition metal ion-doped novel phosphors for possible application in w-LEDs: a review. Lumin 1-30
32. Zhao JY, Wang XG (2019) Preparation, structure and luminescent performance of $Na_2SiF_6$:$Re^{3+}$($Re^{3+}$=$Eu^{3+}$, $Tb^{3+}$,$Ce^{3+}$) powders. Appl Phys A Mater Sci Process 125:178
33. Luo X, Hou Z, Zhou T, Xie RJ (2020) A universal HF-free synthetic method to highly efficient narrowband red-emitting $A_2XF_6$:$Mn^{4+}$ (a = K, Na, Rb, Cs; X = Si, Ge, Ti) phosphors. J Am Ceram Soc 103:1018–1026
34. Yeo BE, Cho YS, Huh YD (2016) Synthesis and photoluminescence properties of a red-emitting phosphor, $K_2SiF_6$:$Mn^{4+}$, for use in three-band white LED applications. Opt Mater 51:50–55
35. Jenkins R, Snyder RL (2012) Introduction to X-ray powder Diffractometry2nd edn. John Wiley & Sons, New York
36. Arianpour F, Cakir Arianpour A, Aali B (2019) Chemical and surface properties of sodium silicofluoride. 2nd international conference on materials science, mechanical and automotive engineering and technology (IMSMATEC'19), Cappadocia, Turkey, June 1165-7
37. Chang SY, Wang C, Sun CC (2019) Relationship between hydrate stability and accuracy of true density measured by helium pycnometry. Int J Pharm 567:118444
38. Buchwald T, Schmandra G, Schützenmeister L, Fraszczak T, Mütze T, Peuker U (2020) Gaseous flow through coarse granular beds: the role of specific surface area. Powder Technol 366:821–831
39. Li H, Li J, Bodycomb J, Patience GS (2019) Experimental methods in chemical engineering: particle size distribution by laser diffraction-PSD. Canadian J Chem Eng 97:2577–2577
40. Kashiwaya Y, Cramb AW (2002) Kinetics of formation and dissociation of $Na_2SiF_6$. Metall Mater Trans B Process Metall Mater Process Sci 33B:129–136
41. Cakir Arianpour A, Arianpour F, Aali B (2020) Microstructural study and thermal behavior of sodium silicofluoride. Int J Eng Res Develop (IJERAD) 12:113–117
42. Soltani N, Canul MIP, Gonzalez LA, Bahrami A (2016) Mechanism and parameters controlling the decomposition kinetics of $Na_2SiF_6$ powder to $SiF_4$. Int J Chem Kinetic 48:379–395
43. Zalkin A, Forrester JD, Templeton DH (1964) The crystal structure of sodium fluosilicate. Acta Cryst 17:1408–1412
44. Liu J, Du N, Wu P, Wang J, Zhang H, Yang D (2012) Large-scale synthesis of water-soluble $Na_2SiF_6$ nanotubes with polyacrylic acid as a surfactant. Mater Res Bull 47:3923–3926
45. Zhigadl ND (2014) Crystal growth of hexagonal boron nitride (hBN) from mg-B-N solvent system under high pressure. J Cryst Growth 402:308–311
46. Rane AV, Kanny K, Abitha VK, Thomas S (2018) Methods for synthesis of nanoparticles and fabrication of nanocomposites. Synthesis of Inorganic Nanomaterials: Advances and Key Technologies, Elsevier 121–139